X-ray phase-contrast imaging at 100 keV on a conventional source

T. Thüring, M. Abis, and M. Stampanoni

Paul Scherrer Institute, Villigen PSI, Switzerland and

Institute for Biomedical Engineering,

Swiss Federal Institute of Technology, Zurich, Switzerland

Z. Wang and C. David

Paul Scherrer Institute, Villigen PSI, Switzerland

(Dated: October 31, 2013)

Abstract

X-ray grating interferometry is a promising imaging technique sensitive to attenuation, refraction and scattering of the radiation. Applications of this technique in the energy range between 80 and 150 keV are still largely unexplored due to the severe technical challenges. Phase-contrast X-ray imaging at such high energies is of relevant scientific and industrial interest, in particular for the investigation of materials with high atomic number or thickness as well as for medical imaging. Here we show the successful implementation of a Talbot-Lau interferometer operated at 100 keV using a conventional X-ray tube and a compact geometry, with a total length of 54 cm. We present edge-on illumination of the gratings to overcome their current fabrication limits as well as curved structures, to match beam divergence and allow large field of views on a short and efficient setup.

X-ray radiography and computed tomography (CT) are standard imaging techniques in materials and life sciences for the nondestructive examination of samples or diagnostic tasks in medicine. The underlying contrast mechanism relies on the different X-ray attenuation properties of different materials or tissue types. The dominant physical effects contributing to attenuation are the photoelectric effect and incoherent (Compton) scattering. Besides attenuation, the wave nature of X-rays reveals another contrast mechanism, which is the phase shift. The interaction contributing to phase shifts is coherent (Rayleigh) scattering [1].

The attenuation and phase shift properties are described by the complex index of refraction $n = 1 - \delta + i\beta$. The imaginary part β is related to the attenuation coefficient by $\mu = 4\pi\beta(\lambda)/\lambda$, while the real part $\delta(\lambda)$ determines the phase shift $\phi = 2\pi\delta(\lambda)/\lambda$

While the attenuation can be measured with an X-ray detector as the reduction of the beam intensity, the phase is not directly observable. Therefore, an optical system is needed to convert the phase shift into intensity modulations.

Phase-sensitive imaging is a desirable modality, as it delivers a complementary source of contrast with respect to absorption by providing direct access to the electron density [1]. Moreover, the combination with attenuation enables the determination of the effective atomic number [2]. An enhanced contrast-to-noise ratio (CNR) in images compared to attenuation for certain materials or tissues [3, 4] has also been demonstrated.

The vast majority of phase-sensitive techniques, including crystal analyzer based [5, 6] or interferometric [7, 8] methods rely on X-ray beams of high spatial and temporal coherence, which is available only at synchrotron sources. Inline phase contrast [9–11] and Talbot interferometry [12–14] need high spatial coherence but are available on polychromatic microfocus sources. Phase-contrast imaging using X-ray beams of low temporal *and* spatial coherence such as conventional low-brilliance X-ray tubes have been demonstrated with coded apertures [15] and Talbot-Lau interferometry [16]. Analyzer-based systems have been recently extended to tube sources [17, 18] but only at energies up to the tungsten K_α line at 60 keV. In addition to phase sensitivity, analyzer-based and Talbot interferometry approaches also provide (with different retrieval mechanisms) information about the integrated local small angle scattering power from microscopic density fluctuations in a specimen [19]. This signal is known under the name of dark-field, scatter or visibility reduction contrast.

High-energy Talbot interferometry has been reported so far using a synchrotron source at nominal energies of 82 keV [20] and 123 keV [21]. Using a low-brilliance X-ray tube,

Talbot-Lau interferometry was applied so far at 60 keV mean energy [22]. Medical imaging applications may benefit from phase contrast at higher energies: chest or abdominal radiography or CT require energies between 100 and 150 kVp. Other potential applications are homeland security or chip failure analysis, which require high energies for the visualization of materials of high density and atomic number.

Here we introduce a method for phase contrast imaging which works on conventional X-ray sources, covers the entire diagnostic X-ray energy range and is compatible with compact imaging arrangements. The approach is based on Talbot-Lau interferometry [16] and employs an edge-on illumination approach for the grating design and arrangement. Our solution removes one on the major hurdle which prevented grating interferometry to be applied at very high X-ray energies so far, namely the fabrication of gratings with high-aspect ratios. The aspect ratio, given by

$$\mathrm{R} = \frac{2h}{p}, \tag{1}$$

where p is the grating period and h the structure height, is normally limited by the fabrication process, usually photolithography [13] or X-ray lithography [23] as grating structures tend to collapse or deform (e.g. due to capillary forces) if the aspect ratio is too high. For a given setup length these parameters depend on the target energy E according to $p \propto 1/\sqrt{E}$ and $h \propto E^3$, and therefore $\mathrm{R} \propto E^{7/2}$ [14]. If at $E = 25\,\mathrm{keV}$ an aspect ratio for the absorption grating around $\mathrm{R} = 30$ is necessary for a reasonable length of the experimental arrangement, it would have to be at least 128 for $E = 100\,\mathrm{keV}$. Moreover, when using a broad spectrum, photons above the design energy should also be efficiently blocked by the gratings, which requires even higher aspect ratios. The largest aspect ratios achieved by current fabrication techniques [24, 25] are around 60.

Our design introduces the edge-on illuminated, circularly aligned structures. Edge-on illumination (Fig. 1), as opposed to face-on illumination, exploits the dimension along the grating lines to form a high aspect ratio of the structures in the direction of the beam. The effective structure height of the grating is then determined by the grating dimension along the grating lines, which essentially allows arbitrarily high aspect ratios.

Increasing the aspect ratio of the gratings typically leads to a reduction of the field of view due to the change of the grating transmission function at high incident angles. In order to overcome this problem, the grating lines are circularly aligned with a radius equal to the distance to the source. This cannot be done with the glancing angle approach [26], and

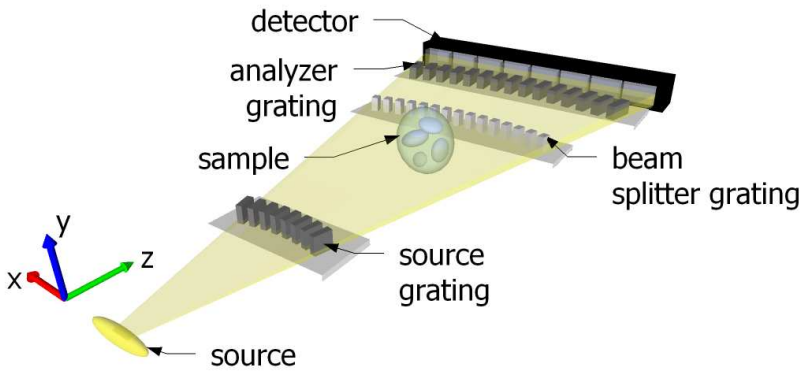

Figure 1. Schematic of a grating interferometer for X-ray energies between 60 and 150 keV in edge-on illumination mode. The aspect ratio is defined by the ratio of the travelling distance along the grating lines and the period and can be arbitrarily long. In order to maximise the field of view, the grating structures are aligned on an arc.

allows an arbitrarily large field-of-view in a fan beam geometry.

The combination of edge-on illumination and circularly aligned structures enables phase-contrast imaging at arbitrary design energies and with a maximum field of view in the horizontal direction (x direction). These advantages come at the expense of a limited field of view in the vertical direction (y direction), which is, depending on the X-ray detector, typically a few pixels. Radiographic 2D imaging can be obtained by scanning the sample or a thin fan beam. The scanning technique has been demonstrated to deliver less dose than the conventional approach based on the illumination of a large area. In digital mammography, for instance, where dose is a critical issue, Philips' MicroDose system combines a scanning approach with an highly collimated fan beam [27]. Thanks to the high collimation, the dose deposited on patients has been reported to be significantly lower than with other instruments based on the illumination of a large area detector [28]. Similarly, for tomographic images, the approach allows single slice CT or full 3D imaging in scanning mode.

Grating design and fabrication is nonstandard and involves a complex mask design, as shown in Fig. 2. Multiple gratings can reside on a silicon chip with their specific structure length and curvature. For the current experiments, a symmetric interferometer with a grating period of $p = 2.8\,\mu\text{m}$ for all gratings has been used. The design energy is 100 keV and the beam splitter grating periodically shifts the phase by zero and π at this energy [13].

Using gold as the phase shifting material, a structure length of $h_1 = 19.8\,\mu\text{m}$ is required. The analyzer grating is an absorption mask for sensing slight changes of the interference pattern generated by the beam splitter [14]. With a structure length of $h_2 = 800\,\mu\text{m}$ it can sufficiently attenuate X-rays up to energies of 160 keV. Beam splitter and analyzer grating are separated at the first fractional Talbot order [29], resulting in an intergrating distance of 158 mm. The source grating splits the relatively large focal spot ($\sim 1\,\text{mm}$) into an array of individually coherent, but mutually incoherent sources [16]. It is also made of gold structures with a length of $h_0 = h_2 = 800\,\mu\text{m}$.

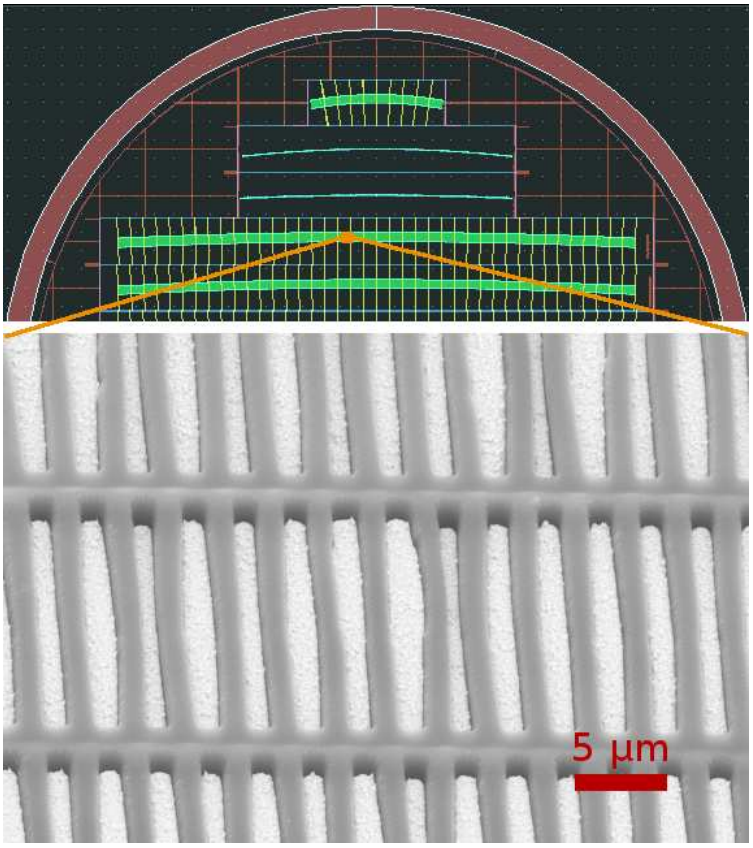

Figure 2. Grating design mask for the edge-on illumination approach and SEM image of the grating. The top part of the 4 inch wafer shows five grating chips. The gratings have different curvatures which are specific to the grating interferometer geometry. The SEM image shows the gold structures and the interrupting bridges that prevent the lamellae from collapsing [25].

Due to the high spectral acceptance [29, 30] of the interferometer (50 keV to more than 160 keV) and the high attenuation efficiencies of the source and analyzer gratings ($> 90\%$ up to 160 keV), the voltage of the X-ray source was set to the maximum of 160 kV. With a

grating structure height of approximately 100 µm, the field of view in the vertical direction is limited to one detector pixel row. In the horizontal direction, the field of view is only limited by the grating size to 30 mm, but wider gratings can be fabricated with this method and the available technology on larger wafers. In addition to the standard components (source, camera, interferometer), two optical slits, one in front of the source grating, the other in front of the camera, were required for the collimation of the beam in the vertical direction.

Fig. 3 shows a radiographic scan of an electronic chip. Several resistors and an integrated circuits are located on different layers on the chip. The images were acquired in scanning mode, using a step size of 100 µm along the y axis. For a better comparison of the magnified phase and attenuation images, the attenuation image has been replaced with the differential attenuation image, which was obtained by digital differentiation. In the attenuation image, the contrast of the soldering points of the integrated circuit is reduced underneath the resistors, while in the phase image, they can clearly be identified. The reduced contrast of the soldering points in the absorption image is due to beam hardening. The spectrum impinging on these soldering point is hardened by the resistors in the upper layer, resulting in lower absorption contrast. Due to the weaker energy dependency of phase shifts ($1/E$ compared to $1/E^3$), phase-contrast images are less sensitive to beam hardening [31], which explains the lower contrast reduction of the soldering points underneath the resistors in the phase image of the chip. This result shows the benefit of the phase nature in high-energy X-ray imaging, which may be useful to identify flaws in multilayered structures such as electronic chips.

Edge-on illuminated grating interferometry finally allows phase contrast imaging to be performed at high energies (> 100 keV) on conventional X-ray sources. With a circular distribution of the gratings, the diffracting and absorbing structures can be matched to the divergent beam, even for very compact geometries. Short, high-energy phase-contrast systems enable the efficient investigation of high-density materials or thick samples, adding information on electron density and integrated small angle scattering power to the conventional absorption based signal. This will improve material discrimination and density sensitivity capabilities in future X-rays or even neutron [32] investigations.

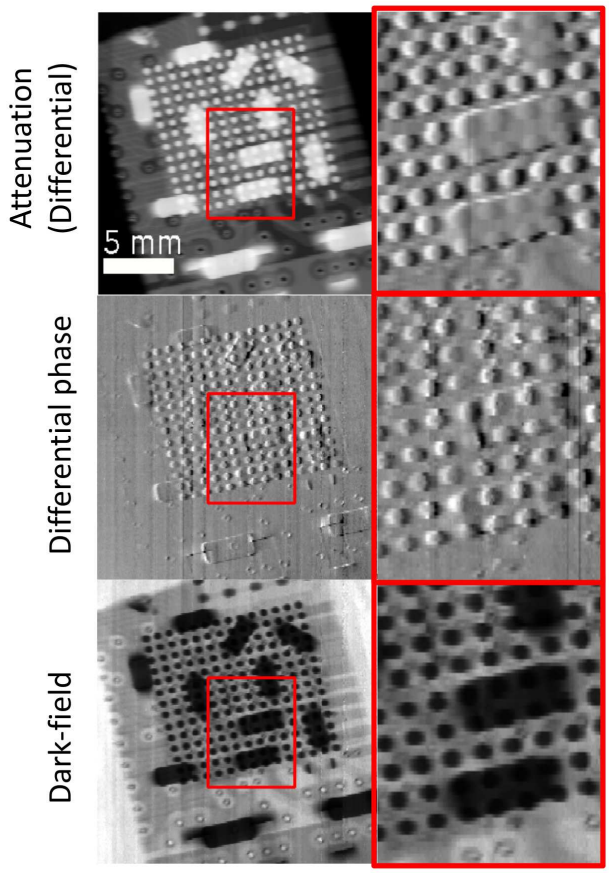

Figure 3. Radiographic scan of an electronic chip. The image was acquired with 24 phase steps per line and an exposure time of 15 s per step. The top right image shows the differential absorption image.

METHODS

Edge-on illuminated gratings were manufactured by Microworks GmbH, Germany, using a LIGA process [25]. Each grating resides on a $5 \times 60\,\mathrm{mm}^2$ silicon chip and several grating chips are fabricated on a single 4 inch silicon wafer. The experimental arrangement for a design energy at 100 keV is a symmetric Talbot-Lau interferometer with a grating period of $p = 2.8\,\mu\mathrm{m}$ for all gratings. The distance from the source grating to the analyzer grating is 32 cm and the source grating is positioned 23 cm away from the source.

The X-ray source is a COMET MXR-160HP/11 X-ray tube with a maximum output voltage of 160 kV. In the experiment, it was set to the maximum voltage. The focal spot size is approximately 1 mm. The detector is a CCD camera from Finger Lakes Instruments.

A cesium iodide (CsI:Ti) scintillator of 600 µm thickness converts the X-rays to visible light and is coupled with an optical lens projecting the image onto the CCD. The effective pixel size is 80 µm. The collimating slit right after the source is 25 µm large, while the second slit before the detector is 100 µm.

In Fig. 3, image acquisition involved 24 phase steps per line and an exposure time of 15 seconds per step. The long exposure times are mostly constrained by the low average visibility of the gratings (5 %). The exposure time was chosen in order to get a low noise in the differential phase image. The signal-to-noise ratio (SNR) is proportional to the visibility and the square root of the exposure time [33]. This implies that the exposure times can easily drop by an order of magnitude as these gratings become comparable in quality to those developed in the last ten years. Smaller regions of these gratings actually exhibit a visibility up to 14 % already, indicating that this goal is reachable as the fabrication becomes more reliable and uniform.

ACKNOWLEDGEMENTS

We thank Gordan Mikuljan, Peter Modregger and István Mohácsi from the Paul Scherrer Institute (PSI), Switzerland, for the work on the mechanical design, the scientific advice, and the SEM images respectively, Joachim Schulz and Marco Walter from Microworks GmbH, Germany, for the competent support on grating design issues, Christian Kottler and Vincent Revol from Centre Suisse d'Electronique et de Microtechnique (CSEM), Switzerland for the fruitful discussions on the design of the system. This work has been partially supported by the Competence Centre for Materials Science and Technology (CCMX) of the ETH Board, Project Nr. 61 and by the ERC Grant ERC-2012-StG 310005-PhaseX.

[1] J. Als-Nielsen and D. McMorrow, *Elements of modern X-ray physics* (2011).

[2] Z. Qi, J. Zambelli, N. Bevins, and G.-H. Chen, Physics in medicine and biology **55**, 2669 (2010).

[3] F. Pfeiffer, O. Bunk, C. David, M. Bech, G. Le Duc, A. Bravin, and P. Cloetens, Physics in medicine and biology **52**, 6923 (2007).

[4] S. A. McDonald, F. Marone, C. Hintermuller, G. Mikuljan, C. David, F. Pfeiffer, M. Stampanoni, and C. Hintermüller, Journal of Synchrotron Radiation **16**, 562 (2009).

[5] T. Davis, D. Gao, T. Gureyev, A. Stevenson, and S. Wilkins, Nature **373**, 595 (1995).

[6] D. Chapman, W. Thomlinson, R. Johnston, D. Washburn, E. Pisano, N. Gmür, Z. Zhong, R. Menk, F. Arfelli, and D. Sayers, Physics in Medicine and Biology **42**, 2015 (1997).

[7] U. Bonse and M. Hart, Applied Physics Letters **6**, 155 (1965).

[8] A. Momose, T. Takeda, Y. Itai, and K. Hirano, Nature Medicine **2**, 473 (1996).

[9] A. Snigirev, I. Snigireva, V. Kohn, S. Kuznetsov, and I. Schelokov, Review of Scientific Instruments **66**, 5486 (1995).

[10] S. Wilkins, T. Gureyev, D. Gao, A. Pogany, and A. Stevenson, Nature **384**, 335 (1996).

[11] P. Cloetens, R. Barrett, J. Baruchel, J. Guigay, and M. Schlenker, Journal of Physics D: Applied Physics **29**, 133 (1996).

[12] P. Cloetens, J. Guigay, C. De Martino, J. Baruchel, and M. Schlenker, Optics letters **22**, 1059 (1997).

[13] C. David, B. Nöhammer, H. Solak, and E. Ziegler, Applied Physics Letters **81**, 3287 (2002).

[14] A. Momose, S. Kawamoto, I. Koyama, Y. Hamaishi, K. Takai, and Y. Suzuki, Japanese Journal of Applied Physics **42**, L866 (2003).

[15] P. Munro, K. Ignatyev, R. Speller, and A. Olivo, Proceedings of the National Academy of Sciences **2012**, 2 (2012).

[16] F. Pfeiffer, T. Weitkamp, O. Bunk, and C. David, Nature Physics **2**, 258 (2006).

[17] I. Nesch, D. P. Fogarty, T. Tzvetkov, B. Reinhart, a. C. Walus, G. Khelashvili, C. Muehleman, and D. Chapman, The Review of scientific instruments **80**, 093702 (2009).

[18] C. Parham, Z. Zhong, D. M. Connor, L. D. Chapman, and E. D. Pisano, "Design and Implementation of a Compact Low-Dose Diffraction Enhanced Medical Imaging System," (2009).

[19] F. Pfeiffer, M. Bech, O. Bunk, P. Kraft, E. Eikenberry, C. Brönnimann, C. Grünzweig, and C. David, Nature Materials **7**, 134 (2008).

[20] M. Willner, M. Bech, J. Herzen, I. Zanette, D. Hahn, J. Kenntner, J. Mohr, A. Rack, T. Weitkamp, and F. Pfeiffer, Optics express **21**, 4155 (2013).

[21] M. Ruiz, I. Zanette, M. Chabior, K. Scherer, J. Mohr, M. Walter, T. Weitkamp, A. Rack, and F. Pfeiffer, Poster, 2nd International Symposium on BioMedical Applications of X-ray Phase Contrast Imaging, Germany, 24/25th January 2013 (2013).

[22] T. Donath, M. Chabior, F. Pfeiffer, O. Bunk, E. Reznikova, J. Mohr, E. Hempel, S. Popescu, M. Hoheisel, M. Schuster, J. Baumann, and C. David, Journal of Applied Physics **106**, 054703 (2009).

[23] J. Mohr, T. Grund, D. Kunka, J. Kenntner, J. Leuthold, J. Meiser, J. Schulz, and M. Walter, **41**, 41 (2012).

[24] C. David, J. Bruder, T. Rohbeck, C. Grünzweig, C. Kottler, A. Diaz, O. Bunk, and F. Pfeiffer, Microelectronic Engineering **84**, 1172 (2007).

[25] J. Kenntner, T. Grund, B. Matthis, M. Boerner, J. Mohr, T. Scherer, M. Walter, M. Willner, A. Tapfer, M. Bech, F. Pfeiffer, I. Zanette, and T. Weitkamp, in *Proceedings of SPIE*, Vol. 7804 (2010) p. 780408.

[26] D. Stutman and M. Finkenthal, Applied physics letters **101**, 91108 (2012).

[27] Åslund, M, *Digital Mammography with a Photon Counting Detector in a Scanned Multislit Geometry*, Ph.D. thesis (2007).

[28] J. M. Oduko, K. C. Young, and A. Burch, in *Digital Mammography*, Lecture Notes in Computer Science, Vol. 6136, edited by J. Martí, A. Oliver, J. Freixenet, and R. Martí (Springer Berlin Heidelberg, 2010) pp. 365–370.

[29] T. Weitkamp, A. Diaz, C. David, F. Pfeiffer, M. Stampanoni, P. Cloetens, and E. Ziegler, Optics Express **13**, 6296 (2005).

[30] T. Thuering, W. Barber, Y. Seo, F. Alhassen, J. Iwanczyk, and M. Stampanoni, Applied Physics Letters **102**, 191113 (2013).

[31] M. Chabior, T. Donath, C. David, O. Bunk, M. Schuster, C. Schroer, and F. Pfeiffer, Medical Physics **38**, 1189 (2011).

[32] C. Grünzweig, F. Pfeiffer, O. Bunk, T. Donath, G. Kühne, G. Frei, M. Dierolf, and C. David, The Review of scientific instruments **79**, 053703 (2008).

[33] R. Raupach and T. G. Flohr, Physics in medicine and biology **56**, 2219 (2011).